A Simple Equation for Regional Climate Change and Associated Uncertainty

FILIPPO GIORGI

Abdus Salam International Centre for Theoretical Physics, Trieste, Italy

(Manuscript received 8 November 2006, in final form 20 June 2007)

ABSTRACT

Simple equations are developed to express regional climate changes for the twenty-first century and associated uncertainty in terms of the global temperature change (GTC) without a dependence on the underlying emission pathways. The equations are applied to regional temperature and precipitation changes over different regions of the world, and relevant parameters are calculated using the latest multimodel ensemble of global climate change simulations. Examples are also shown of how to use the equations to develop probability density functions (PDFs) of regional climate change based on PDFs of GTC. The main advantage of these equations is that they can be used to estimate regional changes from GTC obtained either from simple and intermediate complexity models or from target CO_2 stabilization concentrations.

1. Introduction

It is a remarkable property of the climate change signal simulated by current atmosphere–ocean general circulation models (AOGCMs) that various surface climate variables show regional patterns of change that are very similar across different scenarios and time slices (e.g., Mitchell et al. 1999; Mitchell 2003; Räisänen et al. 2004; Giorgi 2005a). Among such variables are mean surface air temperature and, somewhat to a lesser extent, precipitation. Although the patterns of change are similar across the scenarios, the magnitude of the changes tends to increase monotonically with the greenhouse gas (GHG) forcing and the globally averaged temperature response. This feature underlies the so-called pattern-scaling method (Mitchell et al. 1999; Mitchell 2003), a tool used to produce regional climate change information based on a limited number of global model simulations and scenarios.

What makes this scaling behavior particularly remarkable is that it seems to hold relatively well, even if the emission scenarios have quite different regional features, such as the emission and distribution of atmospheric aerosols. It also seems to hold across a relatively wide range of GHG concentrations and global temperature responses regardless of the underlying emission pathways, especially when the change signal is strong (Giorgi 2005a). Therefore, this robust monotonic dependence would suggest that global temperature change (GTC) might be used as either an independent variable or a predictor for regional climate change.

This would give us a powerful tool for regional climate change prediction in different ways. First, the prediction of regional change would be independent of specific aspects of the underlying emission scenarios and it would only be tied to the global temperature response. This would allow us, for example, to estimate regional changes based on assumptions concerning the GTC without having to account for underlying assumptions on the corresponding emission pathways. Second, results from simple or intermediate complexity models could be used to directly infer regional changes in relevant climatic variables. As a result, for example, probabilistic predictions of regional climate change could be estimated from probabilistic predictions of GTC, based on the use of simplified climate models (e.g., Wigley and Raper 2001; Andronova and Schlesinger 2001; Webster et al. 2003; Mastrandrea and Schneider 2004).

On the basis of these considerations, in this paper a simple equation is developed to express the changes in regional surface climate variables for the twenty-first century in terms of the GTC. In addition, a corresponding equation is developed to relate the uncertainty of the regional change to the GTC. This adds important

Corresponding author address: Filippo Giorgi, Abdus Salam International Centre for Theoretical Physics, Strada Costiera 11, 34014, Trieste, Italy.
E-mail: giorgi@ictp.it

DOI: 10.1175/2007JCLI1763.1

information concerning the predictive value of the regional change equation. The regional climate variables considered here are mean surface air temperature and precipitation, and the parameters of the predictive equations are estimated from the latest set of AOGCM simulations performed in support of the Intergovernmental Panel on Climate Change (IPCC) Fourth Assessment Report, and stored at the Program for Climate Model Diagnosis and Intercomparison (PCMDI; available online at http://www-pcmdi.llnl.gov). This dataset is here referred to as the Multi Global Model Ensemble (MGME).

To illustrate the behavior of the proposed equations, they are applied to twenty-first-century climate change projections for the northern Europe (NEU) and Mediterranean (MED) regions as defined by Giorgi and Bi (2005). The values of relevant parameters for 26 land regions worldwide are, however, also provided. Finally, examples are shown of the use of this methodology to produce probability density functions (PDFs) of regional temperature and precipitation change based on PDFs of GTC.

Section 2 first presents a description of the methods and datasets used in this study. Results from the application of the method to the northern Europe and Mediterranean regions are shown in section 3, while section 4 presents relevant parameters calculated for 26 regions worldwide. Section 5 describes the use of the method to produce PDFs of regional changes, while summary considerations and recommendations for future work are presented in the concluding section 6.

2. Methods and datasets

a. The equations for regional climate change and related uncertainty

We here develop equations in which the change in a regional climate variable is expressed as a function of the GTC (also referred to as ΔTg). Given a regional variable (e.g., surface air temperature T, or precipitation P), its change can be expressed as

$$\Delta(T, P) = [\Delta(T, P)/\Delta\mathrm{Tg}]\Delta\mathrm{Tg} = F_{(T,P)}(\Delta\mathrm{Tg})\Delta\mathrm{Tg}, \quad (1)$$

where T and P are temperature and precipitation, respectively, and $F_{(T,P)}(\Delta\mathrm{Tg})$ is a transfer function that expresses the dependency of the regional temperature or precipitation change on the GTC. The parameters characterizing this function can be found empirically from the MGME (or any other ensemble of AOGCM simulations), as illustrated in the next section. Although $F_{(T,P)}(\Delta\mathrm{Tg})$ can have any functional form, as we will see, in most cases it can be approximated by a constant or a linear function.

Once the transfer function $F_{(T,P)}(\Delta\mathrm{Tg})$ is calculated, we need to estimate the related uncertainty. Here we consider two sources of uncertainty. The first is associated with the different simulations of regional response to global warming by different AOGCMs, and it is referred to as "intermodel uncertainty." This can be measured by the intermodel standard deviation of the simulated $F_{(T,P)}(\Delta\mathrm{Tg})$, which is here referred to as $\sigma_{\mathrm{IM},(T,P)}(\Delta\mathrm{Tg})$, because it is also expressed as a function of the GTC. Previous studies have indicated that the intermodel uncertainty is a dominant source of uncertainty in regional climate change projections (e.g., Kittel et al. 1997; Giorgi and Francisco 2000).

The second source of uncertainty is due to the natural internal variability of the climate system. As discussed by Giorgi (2005a), changes inferred by ensemble means of AOGCM simulations only capture average trends. However, multidecadal variability (or multidecadal "noise") needs to be added to the mean change in order to account for natural multidecadal oscillations, which, especially for variables such as precipitation, indeed can be large compared to the mean trends (Giorgi 2005a). We measure this source of uncertainty [referred to as a $\sigma_{\mathrm{IV},(T,P)}(\Delta\mathrm{Tg})$] with the standard deviation of the changes produced by different realizations with a given model of a given climate change scenario.

The overall uncertainty in the estimate of the transfer function $F_{(T,P)}$ (ΔTg) is thus given by

$$\sigma_{F_{(T,P)}}(\Delta\mathrm{Tg}) = [\sigma_{\mathrm{IM},(T,P)}(\Delta\mathrm{Tg})^2 + \sigma_{\mathrm{IV},(T,P)}(\Delta\mathrm{Tg})^2]^{0.5}, \quad (2)$$

where it is assumed that the two sources of uncertainty are independent of each other. All of the quantities in Eqs. (1) and (2) are calculated from the MGME simulations as illustrated in section 3. The MGME is described in section 2b. Note that all the functions in Eqs. (1) and (2) depend only on the GTC and not on the particular emission pathway that leads to a certain value of GTC. This is the key assumption underlying the use of our proposed approach and it is valid to the extent that the regional patterns of climate change scale with the GTC. Therefore, to the extent that this assumption is valid, the GTC can be considered as an effective predictor for regional temperature and precipitation change. The validity (or, better, the lack of validity) of the scaling assumption is measured by the uncertainty defined by Eq. (2). When this uncertainty is greater than the ensemble average signal, Eq. (1) cannot be expected to have a predictive value.

b. Datasets and illustrative cases

The MGME used here is described in Table 1. It includes 19 models from laboratories around the world spanning a relatively wide range of resolutions, from

TABLE 1. List of models and simulations used in this study. See the PCMDI Web site for more information.

Model	Twentieth century	A1B	A2	B1
BCCR-BCM2–0	1	—	1	1
CCMA-3-T47	5	4	2	4
CNRM-CM3	1	1	1	1
CSIRO-MK3	2	1	1	1
GFDL-CM2–0	3	1	1	1
GFDL-CM2–1	3	1	1	—
GISS-AOM	2	2	—	2
GISS-EH	5	4	—	—
GISS-ER	1	2	1	1
INMCM3	1	1	1	1
IPSL-CM4	1	1	1	1
MIROC3–2II	1	1	-	1
MIROC3–2M	3	3	3	3
MTUB-ECTTO-G	5	3	3	3
MPI-ECIIAM5	3	2	3	3
MRI-CGCM2	5	5	5	5
MCAR-CCSM3	8	6	4	8
MCAR-PCM1	1	3	4	2
UKMO-HADCM3	1	1	1	1

about 1° to 5°. Note that two of the original MGME models are neglected [the Flexible Global Ocean–Atmosphere–Land System (FGOALS) and Beijing Climate Center (BCC) models] because of their poor performance in simulating the climate of the European region, which is used here for our illustrative cases (see below).

The following simulations are available from the MGME dataset (see Table 1): twentieth-century climate, using observed GHG and aerosol forcing (referred to as 20C experiments), and twenty-first-century climate, using GHG and aerosol forcing from the A1B, A2, and B1 emission scenarios of Nakicenovic et al. (2000; referred to as A1B, A2 and B1 experiments, respectively). This set of scenarios spans almost the entire IPCC scenario range, with the B1 experiment being close to the low end of the range (CO_2 concentration of about 550 ppm by 2100), the A2 experiment being close to the high end of the range (CO_2 concentration of about 850 ppm by 2100), and the A1B experiment being close to the middle of the range (CO_2 concentration of about 700 ppm by 2100). As shown in Table 1, many models include multiple realizations for the same experiment, which is important to allow us to estimate the uncertainty associated with the internal model variability.

Monthly data for the MGME experiments are obtained from the PCMDI Web site (see above), and the reader is referred to this online resource for more information on the participating models. To facilitate the model intercomparison, the data are interpolated onto a common 1° grid before being analyzed, which is a grid close to that of the highest resolution models. A common 1° land mask grid is also defined based on the half-degree grid of the observed dataset from the Climatic Research Unit (CRU) of the University of East Anglia (New et al. 2000). This implies that, given that a land-only analysis is presented, some uncertainty is present from the different land definitions at the different model grids. Except for one model, the dataset in Table 1 is the same as that used by Giorgi and Bi (2005).

The changes in climate variables are here calculated for periods of 20 yr. This length of period is sufficient to filter out interannual variability (e.g., resulting from ENSO) but to retain multidecadal variability. The twenty-first century is thus first divided into five consecutive 20-yr periods (2001–20, 2021–40, 2041–60, 2061–80, 2081–2100). Changes are then calculated as the difference between the mean temperature and precipitation for each of these periods and the period of 1961–80, which is chosen as reference because it is the latest 20-yr period in the twentieth century in which the anthropogenic signature is relatively minor (Houghton et al. 2001). Our conclusions, however, do not depend on the choice of the twentieth-century reference period. When multiple realizations of the twentieth-century simulation are available for a given model, the reference period model climatology is calculated as the ensemble average of all available realizations.

We here consider changes in mean surface air temperature and precipitation calculated for the 26 regions, wet seasons, and dry seasons as defined in Table 1 of Giorgi and Bi (2005). For illustrative purposes we discuss in detail results only for the MED (30°–47°N, 10.5°W–37.5°E) and NEU (47°–70°N, 10.5°W–27.5°E) regions. Based on the CRU climatology, in the Mediterranean the wet season is October–March (ONDJFM) and the dry season is April–September (AMJJAS), while over northern Europe AMJJAS is the wet season and ONDJFM is the dry season (Giorgi and Bi 2005). The regional averages include only land points in the CRU-based land mask grid. These two regions were chosen to be particularly representative because they show large changes for both temperature and precipitation and different signs of the precipitation change [positive in northern Europe and negative in the Mediterranean; see below and Giorgi and Bi (2005)]. Indeed, Giorgi (2006) places these regions among the most prominent climate change hot spots.

3. Results for the Mediterranean and northern Europe regions

Figures 1 and 2 show the dependency of northern Europe and Mediterranean wet and dry season temperature and precipitation change on the GTC.

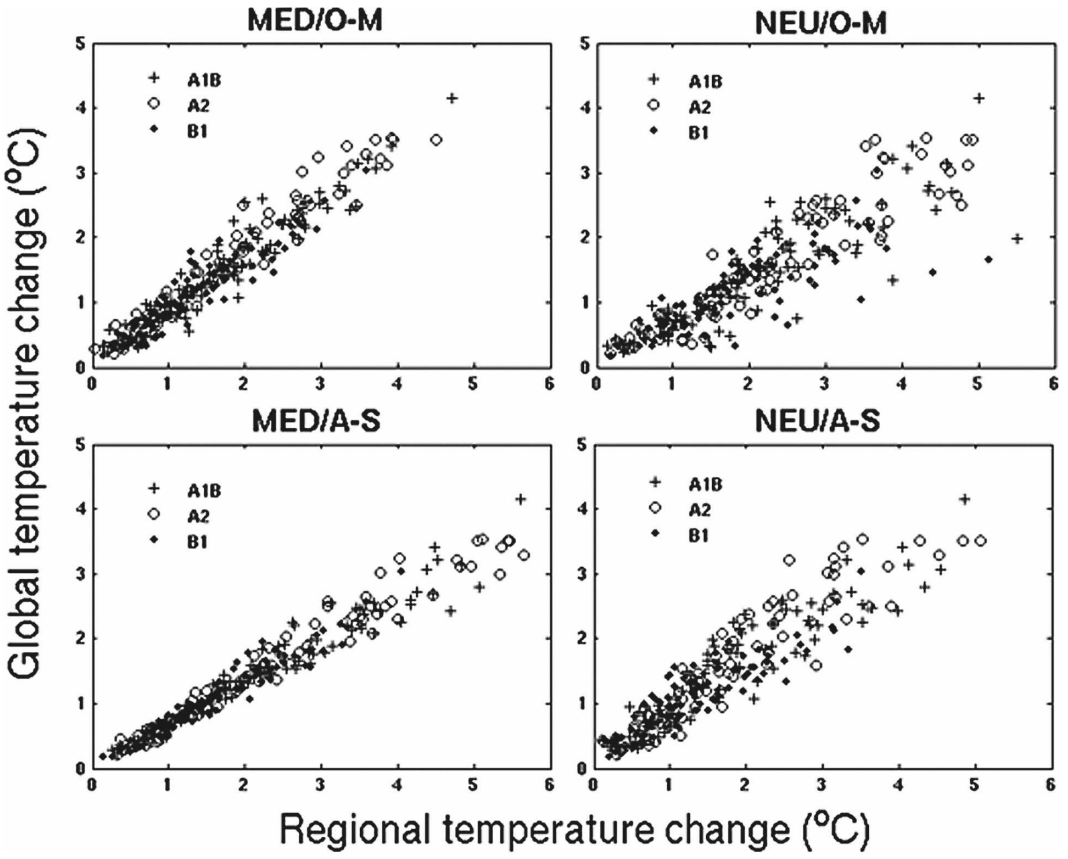

FIG. 1. Scatterplots of global temperature change vs regional temperature change for the MGME ensemble and the four cases: MED O-M (ONDJFM), MED A-S (AMJJAS), NEU O-M (ONDJFM), and NEU A-S (AMJJAS). The changes are calculated for different 20-yr periods of the twenty-first century compared to the reference period of 1961–80 (see text).

Changes for the five 20-yr periods of the twenty-first century with respect to 1961–80 (see section 2b), including all models and scenario simulations, are reported in the scatterplots and, when multiple realizations are available, the ensemble average of the changes is used.

These figures indicate warming in all cases, decreased precipitation over the Mediterranean in both seasons, increased precipitation for the NEU ONDJFM case, and a mixed signal in the NEU AMJJAS case. They give two important messages. First, both for temperature and precipitation, the monotonic dependence of the regional change on the GTC appears to be robust. The only exception is the NEU AMJJAS precipitation change case, in which this monotonic dependence is not present when looking at the overall ensemble, although it is present in individual models. In this case the MGME does not indicate a clear compounded precipitation change signal (Giorgi and Bi 2005), and in fact, as we will see below, the uncertainty is much larger than the signal. The second message is that it is essentially impossible to distinguish between different scenarios in terms of the dependency of the regional change on the GTC. This supports the approach of using the GTC as an independent predictor variable, regardless of the underlying emission pathway.

To verify this assumption we calculated the linear trend values between the GTC and the regional changes of Figs. 1 and 2 for the three scenarios separately and when compounding all of the scenarios together. For temperature the slopes of the trend lines varied by less than 10% between the individual and compounded scenarios. For precipitation they varied by less than 28% in the three cases where a clear relationship is found (MED AMJJAS, MED ONDJFM, NEU ONDJFM), while it was very large for the NEU AMJJAS case in which a clear change signal is not found. This indicates that the basic assumption underlying Eq. (1) is robust for the temperature change, while it is more uncertain for precipitation. The uncertainty related to this assumption is measured by Eq. (2), as shown below.

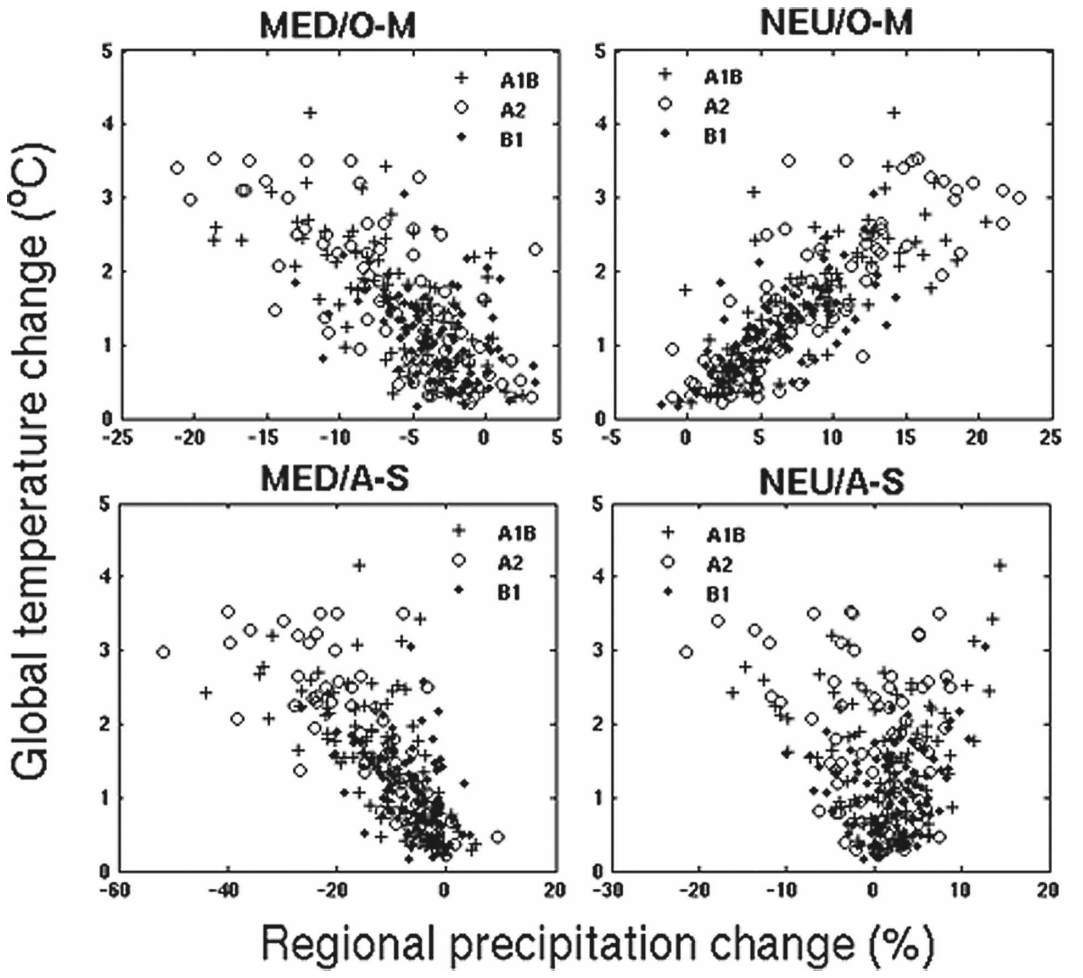

FIG. 2. Same as Fig. 1, but for global temperature change vs regional precipitation change.

The regional changes in Figs. 1 and 2 can be replotted as a function of $\Delta(T, P)/\Delta\mathrm{Tg}$, that is, as a function of $F_{(T,P)}(\Delta\mathrm{Tg})$ in Eq. (1). The resulting scatterplots are shown in Figs. 3 and 4. They show "Christmas tree"–like distributions by which the simulation spread is at a maximum for small values of GTC and decreases with increasing GTC. The Christmas trees are mostly vertical, indicating that, on average, the function $F_{(T,P)}(\Delta\mathrm{Tg})$ remains nearly constant with respect to the GTC, except for the NEU ONDJFM temperature change case (Fig. 3), in which a slight tilt appears. In this case, $F_T(\Delta\mathrm{Tg})$ is evidently a decreasing function of the GTC. The noticeable exception in Figs. 3 and 4 is again the case of the NEU AMJJAS precipitation change in which, as already discussed, the MGME does not give a clear compounded signal.

To calculate the compounded values of $F_{(T,P)}(\Delta\mathrm{Tg})$ and $\sigma_{\mathrm{IM},(\mathrm{T,P})}(\Delta\mathrm{Tg})$ from the MGME the following procedure is used. Given that the number of points in the scatterplots of Figs. 3 and 4 is not large, the full range of simulated GTC is divided into relatively wide bins of 0.5°C width. The average and standard deviation of all the simulated $F_{(T,P)}(\Delta\mathrm{Tg})$ by the individual models falling within each bin are then calculated. This procedure thus provides an estimate of the mean value of $F_{(T,P)}(\Delta\mathrm{Tg})$ and of $\sigma_{\mathrm{IM},(\mathrm{T,P})}(\Delta\mathrm{Tg})$ as a function of the $\Delta\mathrm{Tg}$ of each bin. For our ensemble, at least nine individual model simulations are included in each bin. The mean function $F_{(T,P)}(\Delta\mathrm{Tg})$ and intermodel uncertainty $\sigma_{\mathrm{IM},(\mathrm{T,P})}(\Delta\mathrm{Tg})$ resulting from these calculations at each $\Delta\mathrm{Tg}$ bin for the Mediterranean and northern Europe cases are given in Tables 2 and 3.

Note that the calculations are carried out only for values of $\Delta\mathrm{Tg}$ greater than 0.5°C, because the model spread is much larger than the actual signal for smaller changes. Also, in the MGME simulations analyzed here the value of $\Delta\mathrm{Tg}$ for the 20-yr periods considered does not exceed 4°C. Strictly speaking, our approach can thus be considered to be valid only for the GTC range of 0.5°–4°C.

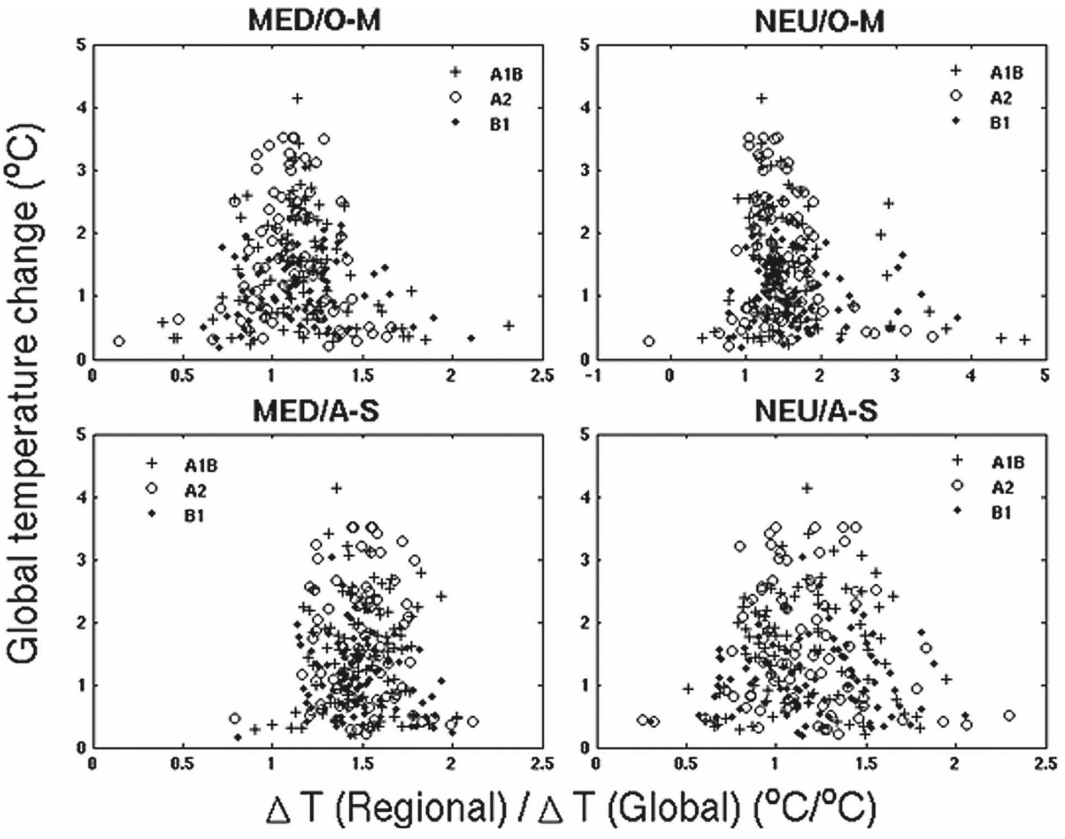

FIG. 3. Same as Fig. 1, but for global temperature change vs $\Delta T(\text{reg})/\Delta\text{Tg}$.

Table 2 first shows that, for temperature, the function $F_T(\Delta\text{Tg})$ is essentially constant for the NEU AMJJAS (~1.16°C/°C), MED ONDJFM (~1.08°C/°C), and MED AMJJAS (~1.48°C/°C) cases, while it shows a decreasing trend with increasing ΔTg for NEU ONDJFM. The latter is *possibly* due to an incremental decrease of snow cover over northern Europe as the global warming increases. This causes a decrease in the snow–albedo feedback process and thus a decrease in the regional temperature sensitivity to global warming. The largest values of $F_T(\Delta\text{Tg})$ occur for the warm–dry season over the Mediterranean and reflect the pronounced sensitivity of summer Mediterranean climate to global warming found in previous studies (Giorgi and Bi 2005; Giorgi 2006).

Concerning the intermodel temperature standard deviation $\sigma_{\text{IM},T}(\Delta\text{Tg})$, we notice two features. First, the values of $\sigma_{\text{IM},T}(\Delta\text{Tg})$ are much smaller than those of $F_T(\Delta\text{Tg})$, which is an indication of the robustness of the simulated temperature change signals. Second, in all regional and seasonal cases we find a decreasing trend of $\sigma_{\text{IM},T}(\Delta\text{Tg})$, with ΔTg. In other words, relative to the GTC, the models tend to agree more as the change signal increases (while in absolute terms the opposite is true). This is consistent with the finding by Giorgi (2005a) that the scaling approach increases in validity as the magnitude of the forcing and change signal increases.

Turning our attention to precipitation (Table 3), we find roughly constant values of bin-averaged $F_P(\Delta\text{Tg})$ in both seasons over the Mediterranean, both showing decreases (~−3.59%/°C in ONDJFM and ~−7.63%/°C in AMJJAS). Over northern Europe we find a decreasing trend of $F_P(\Delta\text{Tg})$ with increasing ΔTg in NEU ONDJFM and large variations of values in NEU AMJJAS when, as mentioned above, the change signal by the MGME is not consistent across models. The values of $\sigma_{\text{IM},P}(\Delta\text{Tg})$ for precipitation show a consistent decreasing trend with increasing ΔTg. For NEU ONDJFM, MED ONDJFM, and MED AMJJAS, the values of $\sigma_{\text{IM},P}(\Delta\text{Tg})$ are comparable to those of $F_P(\Delta\text{Tg})$ for small ΔTg, indicating that the multimodel signal is not large compared to intermodel noise. For large ΔTg, however, $\sigma_{\text{IM},P}(\Delta\text{Tg})$ becomes substantially smaller than $F_P(\Delta\text{Tg})$, indicating an increased robustness of the multimodel signal. The exception in Table 3 is the NEU AMJJAS case, for which the intermodel uncertainty is always larger than the multimodel signal.

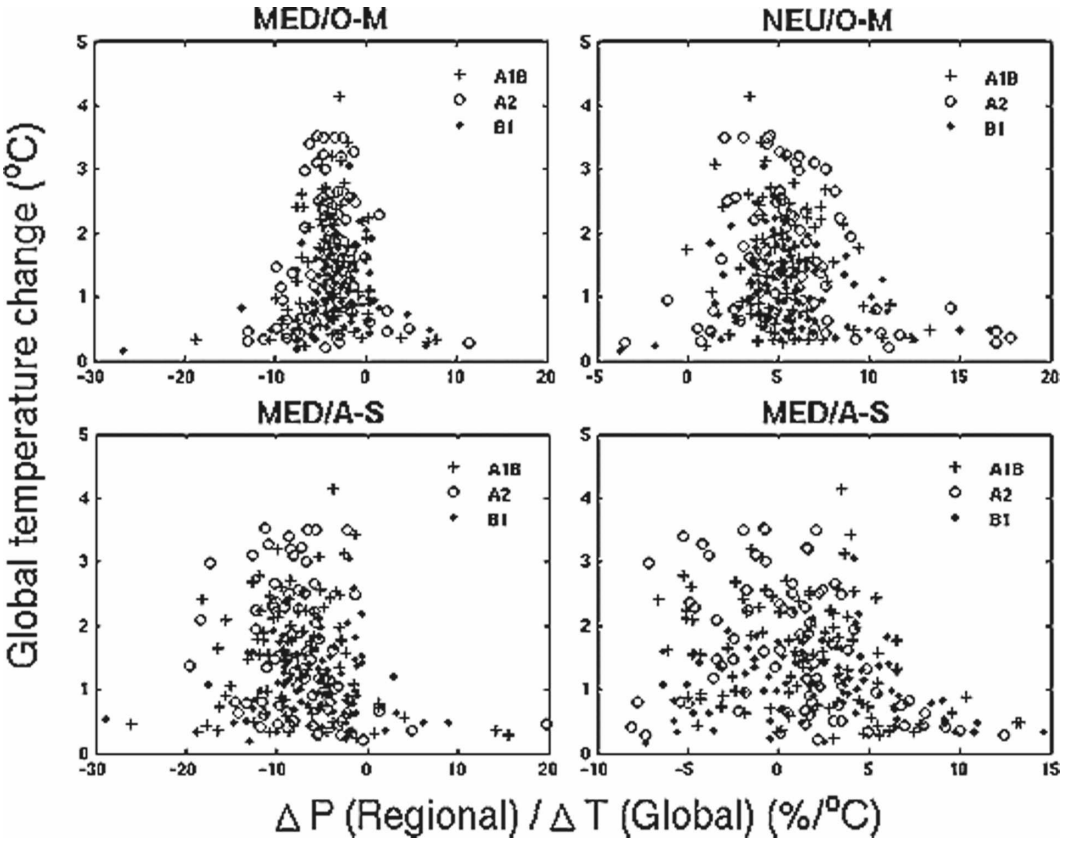

FIG. 4. Same as Fig. 1, but for global temperature change vs $\Delta P(\text{reg})/\Delta\text{Tg}$.

As mentioned, the second source of uncertainty we consider here is that due to internal multidecadal variability as measured by the standard deviation $\sigma_{\text{IV},(T,P)}(\Delta\text{Tg})$ (see section 2). This quantity is calculated as follows. Each model simulation falling in each GTC bin is first identified. If, for a given model scenario simulation, more than one realization is available, the anomaly of the change for each realization is calculated as compared to the ensemble average change for that model. This produces a set of anomalies asso-

TABLE 2. Values of the temperature functions $F_T(\Delta\text{Tg})$, $\sigma_{\text{IM},T}(\Delta\text{Tg})$, and $\sigma_{\text{IV},T}(\Delta\text{Tg})$ for different ΔTg bins in the NEU ONDJFM, NEU AMJJAS, MED ONDJFM, and MED ONDJFM cases (see text). Units: °C/°C.

ΔTg	0.5°–1.0°C	1.0°–1.5°C	1.5°–2.0°C	2.0°–2.5°C	2.5°–3.0°C	3.0°–3.5°C	3.5°–4.0°C
			$F_T(\Delta\text{Tg})$				
NEC ONDJFM	1.72	1.56	1.54	1.50	1.41	1.40	1.21
NEC AMJJAS	1.16	1.15	1.13	1.14	1.15	1.18	1.18
MED ONDJFM	1.08	1.08	1.10	1.08	1.09	1.08	1.00
MED AMJJAS	1.50	1.48	1.47	1.47	1.49	1.48	1.49
			$\sigma_{\text{IM},T}(\Delta\text{Tg})$				
NEU ONDJFM	0.47	0.35	0.31	0.28	0.30	0.20	0.12
NEC AMJJAS	0.31	0.23	0.22	0.24	0.20	0.19	0.19
MED ONDJFM	0.20	0.15	0.12	0.13	0.11	0.12	0.06
MED AMJJAS	0.27	0.20	0.18	0.18	0.18	0.19	0.14
			$\sigma_{\text{IV},T}(\Delta\text{Tg})$				
NEU ONDJFM	0.38	0.22	0.13	0.11	0.07	0.05	0.04
NEC AMJJAS	0.18	0.13	0.09	0.08	0.04	0.04	0.06
MED ONDJFM	0.16	0.11	0.09	0.07	0.04	0.03	0.03
MED AMJJAS	0.16	0.13	0.11	0.12	0.04	0.03	0.03

TABLE 3. Values of the precipitation functions $F_P(\Delta Tg)$, $\sigma_{IM,P}(\Delta Tg)$, and $\sigma_{IV,P}(\Delta Tg)$ for different ΔTg bins in the NEU ONDJFM, NEU AMJJAS, MED ONDJFM, and MED ONDJFM cases (see text). Units: %/°C.

ΔTg	0.5°–1.0°C	1.0°–1.5°C	1.5°–2.0°C	2.0°–2.5°C	2.5°–3.0°C	3.0°–3.5°C	3.5°–4.0°C
			$F_P(\Delta Tg)$				
NEU ONDJFM	6.49	5.66	5.63	5.38	5.07	5.61	4.30
NEU AMJJAS	3.26	2.07	0.89	1.30	0.32	−0.76	0.25
MED ONDJFM	−3.78	−3.23	−3.52	−3.50	−3.41	−4.25	−3.42
MED AMJJAS	−7.56	−7.48	−7.70	−7.99	−7.94	−8.23	−6.47
			$\sigma_{IM,P}(\Delta Tg)$				
NEU ONDJFM	4.19	2.48	2.06	1.96	1.56	2.31	1.50
NEU AMJJAS	3.72	3.26	2.86	2.17	2.83	3.58	3.20
MED ONDJFM	3.86	3.04	2.13	1.89	1.99	1.55	1.54
MED AMJJAS	7.32	5.05	3.83	4.01	3.63	4.36	3.41
			$\sigma_{IV,P}(\Delta Tg)$				
NEU ONDJFM	2.35	1.32	0.80	0.80	0.59	0.52	0.34
NEU AMJJAS	2.47	1.40	1.01	0.77	0.66	0.30	0.28
MED ONDJFM	3.47	1.90	1.45	1.11	1.04	0.88	0.60
MED AMJJAS	3.28	2.21	1.70	1.19	1.20	0.43	0.74

ciated with each simulation for models with multiple realizations of a given scenario. These anomalies are then squared and added including all different model simulations falling within a GTC bin. Finally, $\sigma_{IV,(T,P)}(\Delta Tg)$ is approximated by the root-mean-square of this value. In other words, $\sigma_{IV,(T,P)}(\Delta Tg)$ is defined by the root-mean-square anomaly of the model realizations with respect to the corresponding ensemble average for that model falling within a given GTC bin. Only models for which more than one realization is available are included in the root-mean-square average. In addition, in order to produce values comparable to those of $\sigma_{IV,(T,P)}(\Delta Tg)$, each anomaly is normalized by the respective simulated GTC. It should be emphasized that this procedure gives only a first-order estimate of the internal variability, limited by the availability of a small number of multiple realizations, and evidently gives more weight to the models that completed larger ensembles of realizations.

Tables 2 and 3 summarize the values of $\sigma_{IV,(T,P)}(\Delta Tg)$ for temperature and precipitation change in the northern Europe and Mediterranean cases. We first note that in all cases $\sigma_{IV,(T,P)}(\Delta Tg)$ decreases with ΔTg. This is essentially because of the normalization by ΔTg, because the actual values of the root-mean-square multidecadal anomalies do not vary much with increasing ΔTg. This implies that the multidecadal variability does not change much throughout the twenty-first century MGME simulations. Tables 2 and 3 show that the values of $\sigma_{IV,(T,P)}(\Delta Tg)$ are consistently lower than those of $\sigma_{IM,(T,P)}(\Delta Tg)$, both for temperature and precipitation, and especially for large ΔTg. This indicates that the uncertainty due to internal variability is lower than the intermodel uncertainty, a result consistent with assessments of previous generations of AOGCM simulations (e.g., Giorgi and Francisco 2000). The contribution of internal variability is however not insignificant, especially for precipitation at relatively small ΔTg.

Finally, the temperature and precipitation changes along with the related total uncertainty estimates (Eq. 2) for the NEU ONDJFM, NEU AMJJAS, MED ONDJFM, and MED AMJJAS cases are reported as a function of ΔTg in Figs. 5 and 6. Also shown are the corresponding least squares fit lines. For temperature change the total uncertainty estimates [as measured by $\sigma_{F,T}(\Delta Tg)$] are much lower than the values of the transfer function $F_T(\Delta Tg)$ in all cases. In three of the cases the function $F_T(\Delta Tg)$ is essentially a constant, while in the NEU ONDJFM case it is a decreasing function of ΔTg that is well approximated by a linear fit.

For precipitation (Fig. 6), in all cases, $\sigma_{F,P}(\Delta Tg)$ decreases with increasing ΔTg, while the value of $F_P(\Delta Tg)$ decreases with ΔTg in the northern Europe cases but is essentially constant in the Mediterranean cases. In the NEU AMJJAS case the magnitude of the uncertainty estimate $\sigma_{F,P}(\Delta Tg)$ is actually larger than the magnitude of the transfer function $F_P(\Delta Tg)$ for all values of ΔTg, while the opposite mostly occurs in the other cases.

We thus see that, especially for precipitation, there is a substantial case-to-case variability in the shape of the function $F_{(T,P)}(\Delta Tg)$ and in its relative magnitude compared to the corresponding uncertainty estimate $\sigma_{F,(T,P)}(\Delta Tg)$. Figures 5 and 6 also show that a linear fit provides a reasonably good first-order approximation of the ΔTg dependence of $F_{(T,P)}(\Delta Tg)$ and $\sigma_{F,(T,P)}(\Delta Tg)$, at least in the range examined here (0.5°–4°C). This fit is especially good for temperature, while for precipitation it underestimates the uncertainty at low ΔTg and overestimates it at high ΔTg. In this latter case a higher-

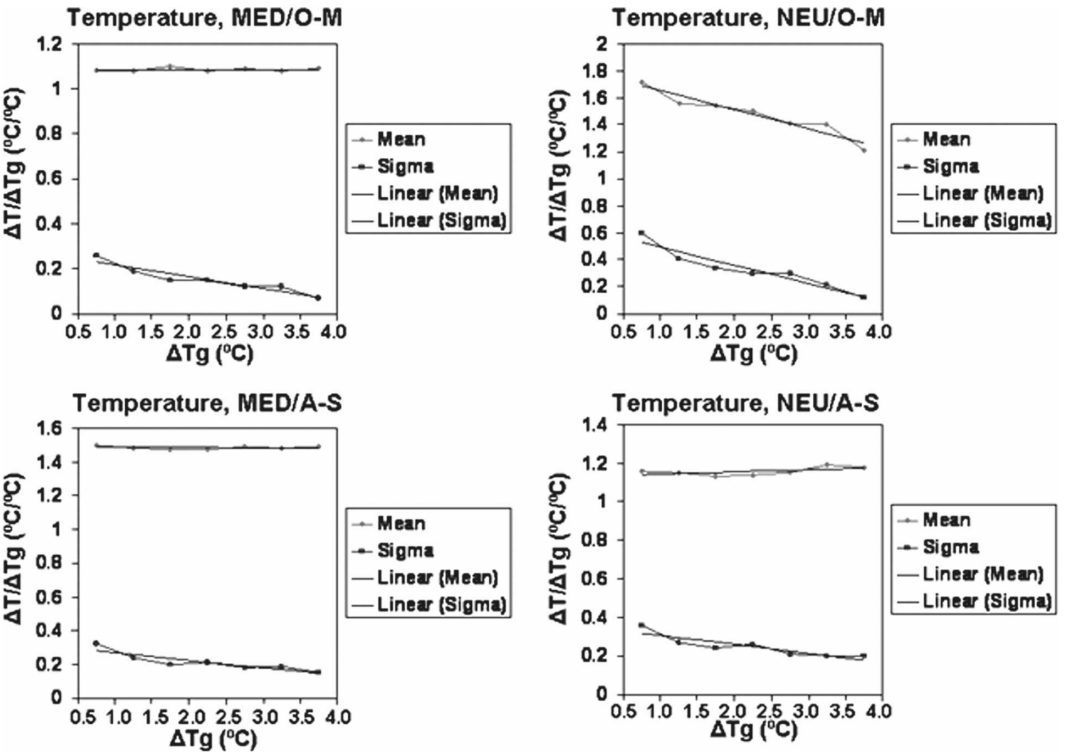

FIG. 5. Values of the mean function $F_T(\Delta\text{Tg})$ (mean) and of $\sigma_{F,T}(\Delta\text{Tg})$ (sigma) at the different ΔTg bins for the MGME ensemble and the four cases in Fig.1. The values are associated to the centers of the bins. Also shown are the corresponding best-fit trend lines.

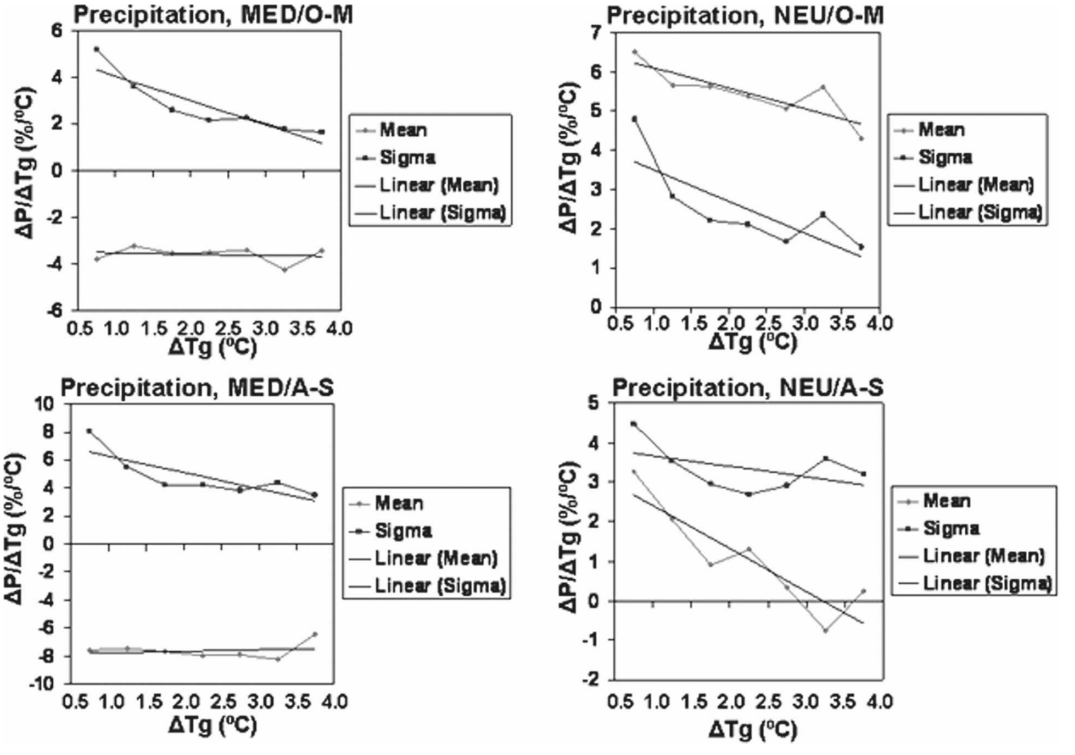

FIG. 6. Same as Fig. 5, but for $F_P(\Delta\text{Tg})$ (mean) and of $\sigma_{F,P}(\Delta\text{Tg})$ (sigma).

order polynomial fit or an exponential fit might be more accurate.

4. Parameter calculations for other regions

In the previous section we have seen that the transfer function $F_{(T,P)}(\Delta Tg)$ and uncertainty estimate $\sigma_{F,(T,P)}(\Delta Tg)$ can be approximated either by a constant or by a linear function of ΔTg. We calculated these values for all the 26 regional wet and dry season cases defined by Giorgi and Bi (2005; the reader is referred thereto for the definitions of regions and wet and dry seasons).

The results are reported in Tables 4 and 5, which show a number of parameters. First, the cases in which a trend in $F_{(T,P)}(\Delta Tg)$ or $\sigma_{F,(T,P)}(\Delta Tg)$ is found to be statistically significant at the 90% confidence level according to a two-tailed t test are identified. In these cases, $F_{(T,P)}(\Delta Tg)$ and $\sigma_{F,(T,P)}(\Delta Tg)$ are expressed by formulas of the type $a + (b\Delta Tg)$, and Tables 4 and 5 report the values of $[a + (b \times 0.5)]$ [i.e., the intercepts of the F and σ functions at the value $\Delta Tg = 0.5$, because Eqs. (1) and (2) are valid only for ΔTg greater than 0.5] and b (i.e., the slope of the trend line). When a statistically significant trend is not present, $F_{(T,P)}(\Delta Tg)$ and $\sigma_{F,(T,P)}(\Delta Tg)$ are assumed to be constant and equal to their average value across the entire ΔTg range. For these cases this average value is reported in Tables 4 and 5. Finally, for precipitation, cases are highlighted in bold for which the mean value of $F_P(\Delta Tg)$ across the ΔTg range is greater than the mean value of $\sigma_{F,P}(\Delta Tg)$, that is, when the signal-to-noise ratio is relatively large. For temperature this is always the case.

Before we analyze the results of Tables 4 and 5, it should be mentioned that the underlying hypothesis of this work (i.e., that the relation of the regional change on the GTC does not depend on the underlying emission scenario) was evaluated for all cases in Tables 4 and 5. As in section 3, this was done by comparing the linear trend lines calculated for the different scenarios separately and for all scenarios compounded together. For temperature we again found that the line slopes varied by less than 10% in the vast majority of cases, showing the solidity of this assumption. For precipitation, the differences were less than 30% for the bold cases in Tables 4 and 5, that is, for the cases in which the signal is greater than the noise. This shows the greater uncertainty present in the use of Eq. (1) for regional precipitation compared to temperature.

Table 4 shows that for temperature $\sigma_{F,T}(\Delta Tg)$ is always characterized by a significant and negative dependence on ΔTg. This indicates that the uncertainty of the predictive regional temperature equation always de-

TABLE 4. Values of the temperature parameters (see text): $F_T(0.5)$; trend in $F_T(\Delta Tg)$, b_F; mean value of $F_T(\Delta Tg)$, F_M; $\sigma_{F,T}(0.5)$; and trend in $\sigma_{F,T}(\Delta Tg)$, b_σ. Units: °C/°C for the function F and °C/°C^2 for the trends. Parameter values are reported for the regional cases defined by Giorgi and Bi (2005; see therein for the definition of the regions). May–October (MJJASO), November–April (NDJFMA), February–July (FMAMJJ), August–January (ASONDJ), June–November (JJASON), and December–May (DJFMAM).

	$F_T(0.5)$	b_F	F_M	$\sigma_{F,T}(0.5)$	b_σ
NEU MJJASO			1.16	0.33	−0.046
NEU NDJFMA	1.72	−0.142		0.56	−0.132
MED ONDJFM			1.08	0.24	−0.052
MED AMJJAS			1.48	0.29	−0.046
NEE MJJASO			1.39	0.43	−0.068
NEE NDJFMA			1.99	0.72	−0.147
NAS MJJASO	1.37	0.027		0.37	−0.044
NAS NDJFMA			1.97	0.50	−0.075
CAS NDJFMA			1.30	0.32	−0.070
CAS MJJASO	1.64	−0.038		0.34	−0.063
TIB AMJJAS			1.43	0.28	−0.047
TIB ONDJFM			1.54	0.34	−0.067
EAS AMJJAS	1.11	0.40		0.24	−0.034
EAS ONDJFM			1.27	0.36	−0.082
SAS MJJASO			1.07	0.24	−0.032
SAS NDJFMA			1.28	0.27	−0.050
SEA AMJJAS			0.95	0.15	−0.027
SEA ONDJFM	0.89	0.013		0.16	−0.031
NAU NDJFMA	1.15	0.018		0.29	−0.041
NAU MJJASO	1.30	−0.029		0.27	−0.049
SAU MJJASO	1.05	−0.037		0.26	−0.051
SAU NDJFMA	1.05	0.013		0.26	−0.045
SAH NDJFMA			1.29	0.24	−0.055
SAH MJJASO	1.57	−0.035		0.27	−0.044
WAF MJJASO			1.22	0.30	−0.045
WAF NDJFMA			1.23	0.24	−0.017
EAF MJJASO			1.21	0.26	−0.018
EAF NDJFMA			1.20	0.22	−0.027
EQF FMAMJJ			1.11	0.22	−0.027
EQF ASONDJ			1.08	0.23	−0.026
SQF NDJFMA	1.12	0.025		0.20	−0.026
SQF MJJASO			1.28	0.28	−0.039
SAF ONDJFM	1.17	0.015		0.26	−0.039
SAF AMJJAS	1.23	−0.008		0.27	−0.041
ALA JJASON			1.35	0.38	−0.060
ALA DJFMAM	1.83	−0.020		0.63	−0.131
GRL JJASON			1.51	0.38	−0.043
GRL DJFMAM			1.87	0.55	−0.115
WNA ONDJFM	1.19	0.038		0.38	−0.071
WNA AMJJAS			1.53	0.37	−0.058
CAN AMJJAS			1.54	0.40	−0.042
CAN ONDJFM			1.39	0.41	−0.085
ENA AMJJAS			1.37	0.30	−0.036
ENA ONDJFM	1.48	−0.024		0.39	−0.082
CAM MJJASO	1.22	0.022		0.25	−0.037
CAM NDJFMA	1.08	0.025		0.25	−0.053
AMZ NDJFMA	1.12	0.028		0.22	−0.021
AMZ MJJASO	1.27	0.031		0.24	−0.018
CSA ONDJFM	1.07	0.024		0.25	−0.036
CSA AMJJAS			1.04	0.18	−0.028
SSA AMJJAS	0.73	−0.015		0.21	−0.050
SSA ONDJFM	0.84	−0.027		0.27	−0.060

TABLE 5. Values of the precipitation parameters (see text): $F_P(0.5)$; trend in $F_P(\Delta\text{Tg})$, b_F; mean value of $F_P(\Delta\text{Tg})$, F_M; $\sigma_{F,P}(0.5)$; trend in $\sigma_{F,P}(\Delta\text{Tg})$, b_σ; and mean value of $\sigma_{F,P}(\Delta\text{Tg})$, σ_M. Units are %/°C for the function F and %/°C^2 for the trends. Parameter values are reported for the regional cases defined by Giorgi and Bi (2005; see therein for the definition of the regions). Bold cases are those in which the mean value of F is greater than the mean value of σ.

Case	$F_P(0.5)$	b_F	F_M	$\sigma_{F,P}(0.5)$	b_σ	σ_M
NEU MJJASO	2.95	−1.089				3.34
NEU NDJFMA	6.35	−0.519		3.90	−0.802	
MED ONDJFM			−3.59	4.55	−1.039	
MED AMJJAS			−7.62	6.83	−1.159	
NEE MJJASO	3.94	−0.827		5.28	−0.929	
NEE NDJFMA			7.24	3.62	−0.754	
NAS MJJASO			4.17			1.86
NAS NDJFMA	8.47	0.621		3.48	−0.585	
CAS NDJFMA			−0.46	5.25	−1.172	
CAS MJJASO			−3.00	8.48	−1.387	
TIB AMJJAS			3.15			2.91
TIB ONDJFM			5.84	3.66	−0.427	
EAS AMJJAS	1.25	0.653		3.40	−0.598	
EAS ONDJFM	1.11	0.561		5.53	−0.70	
SAS MJJASO			3.50	5.07	−0.934	
SAS NDJFMA	−3.30	0.918		8.71	−1.684	
SEA AMJJAS	1.86	0.197		3.04	−0.401	
SEA ONDJFM	0.79	0.493		2.77	−0.376	
NAU NDJFMA			2.14	8.30	−1.703	
NAU MJJASO			−3.72	16.02	−3.776	
SAU MJJASO			−4.74	9.13	−2.035	
SAU NDJFMA	3.58	−0.976		9.37	−1.961	
SAH NDJFMA			−6.17	12.68	−2.822	
SAH MJJASO			−0.11	26.19	−5.359	
WAF MJJASO			−0.61	4.19	−0.603	
WAF NDJFMA			−0.12		3.81	
EAF MJJASO			1.70		3.60	
EAF NDJFMA	2.31	0.582		6.25	−1.057	
EQF FMAMJJ	1.89	1.151		5.20	−0.740	
EQF ASONDJ	2.74	0.874				3.70
SQF NDJFMA			0.44	2.90	−0.555	
SQF MJJASO			−3.08	6.78	−1.276	
SAF ONDJFM			−0.25	5.61	−0.886	
SAF AMJJAS			−4.55	7.82	−1.674	
ALA JJASON	3.92	0.440		2.90	−0.368	
ALA DJFMAM	5.72	0.469		3.18	−0.530	
GRL JJASON			4.97	2.20	−0.368	
GRL DJFMAM	6.37	0.522		4.29	−0.780	
WNA ONDJFM			1.88	5.47	−1.101	
WNA AMJJAS	−4.34	0.648		6.45	−10.368	
CAN AMJJAS	0.74	−0.915				4.63
CAN ONDJFM	2.40	−0.438		4.85	−0.685	
ENA AMJJAS	3.00	−0.869				2.71
ENA ONDJFM			4.01	4.94	−0.906	
CAM MJJASO	−2.71	−0.620		5.59	−0.339	
CAM NDJFMA	−7.17	0.337				5.52
AMZ NDJFMA	2.05	−0.331			2.66	
AMZ MJJASO	−1.23	−0.379			4.19	
CSA ONDJFM			1.22			3.35
CSA AMJJAS			−1.50	7.84	−1.460	
SSA AMJJAS	0.39	−0.299		2.97	−0.606	
SSA ONDJFM	−5.12	0.564		4.14	−0.828	

creases with the magnitude of the signal. Quite a wide range of trend values is found, from −0.018°C/°C to −0.147°C/°C. In particular, the trend is largest in Northern Hemisphere high-latitude regions [northeastern Europe (NEE), Alaska (ALA), northern Europe (NEU), and Greenland (GRL)] during the cold seasons. This is *possibly* tied to the progressive reduction of snow and ice cover, which leads to a decrease in intermodel uncertainty. Note also that over these regions the ΔTg = 0.5 uncertainty intercept is also the highest, indicating a large uncertainty in the regional temperature sensitivity to global change.

In terms of the temperature transfer function $F_T(\Delta\text{Tg})$ (Table 4), which has essentially the same meaning as the regional warming amplification factor of Giorgi and Bi (2005), we can see a relatively equal split of regional cases with and without a statistically significant trend. A majority of constant $F_T(\Delta\text{Tg})$ values is found over the European, Asian, African, and North American regions, while the presence of trends prevails over the Australian, and Central and South American regions. The values of $F_T(\Delta\text{Tg})$ are generally largest over Northern Hemisphere high-latitude regions in the cold season, indicating a maximum climate response over these regions. Different from the case of $\sigma_{F,T}(\Delta\text{Tg})$, we find trends in $F_T(\Delta\text{Tg})$ of both positive and negative signs.

In the case of precipitation (Table 5), we find a more varied picture. First of all, only in about 40% of the cases the average value of $F_P(\Delta\text{Tg})$ is greater than that of $\sigma_{F,P}(\Delta\text{Tg})$. This indicates that in the majority of cases the uncertainty in the prediction of regional climate change is larger than the compounded signal. This is for a number of reasons: the small magnitude of the precipitation change signal, the large interdecadal variability of regional precipitation, the inconsistency of regional precipitation projections across models, and the need of large ensembles to extract the change signal from the underlying multidecadal and intermodel noise. Among the regions where the magnitude of $F_P(\Delta\text{Tg})$ is greater than that of $\sigma_{F,P}(\Delta\text{Tg})$, we find the European regions; Tibet and the north, East, and South Asia regions; eastern equatorial Africa; Alaska; Greenland; and the eastern North America, Central America, and southern South America regions.

Similarly to the case of temperature, the trend in $\sigma_{F,P}(\Delta\text{Tg})$ is always negative, indicating a relative decrease of uncertainty with increasing ΔTg, except for a few cases of constant values (i.e., trends not statistically significant). Also, the trends in $F_P(\Delta\text{Tg})$ are of both positive and negative signs, and this sign does not appear to be specifically tied to the sign of the precipitation change signal itself. Among the regions with the largest values of $F_P(\Delta\text{Tg})$, we highlight the northern high-latitude regions (positive values in both wet and dry seasons), the Mediterranean and Central America (large negative values especially in the dry seasons), eastern equatorial Africa (increases in both long and short rainy seasons), and southern South America (large decrease in the dry–cold season).

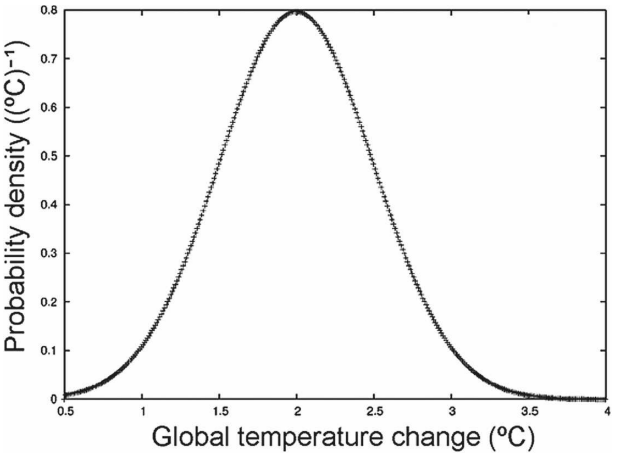

FIG. 7. Global temperature change PDF used for the illustrative applications shown in section 5. The PDF is a normal distribution with central value at 2°C and std dev of 0.5°C.

5. An example of application to the probabilistic prediction of regional climate change

In this section we illustrate how Eqs. (1) and (2) can be applied to produce PDFs of regional climate change from PDFs of GTC. The advantage of this type of application, for example, is that it can be used to produce regional climate PDFs from GTC PDFs generated by large ensembles of simple or intermediate complexity models. This would allow us to better cover the climate change phase space defined by ensembles of models and scenarios and by the internal variability of the climate system (e.g., Giorgi 2005b). In this regard, we base our illustrative application on the GTC PDF shown in Fig. 7. This is a normal PDF distribution close to (although not the same as) the one referred to as "2070" in Fig. 4 of Wigley and Raper (2001), which was obtained using a very large ensemble of simulations with a highly simplified climate system model. Note that the distribution on Fig. 7 fits nicely within the GTC range found in the MGME and used to calculate the transfer functions in this work.

We show two sets of applications. In the first, the transfer function $F_{(T,P)}(\Delta\text{Tg})$ is used without consideration of the associated uncertainty, while in the second the uncertainty is accounted for by use of the function $\sigma_{F,(T,P)}(\Delta\text{Tg})$. For illustrative purposes, these functions

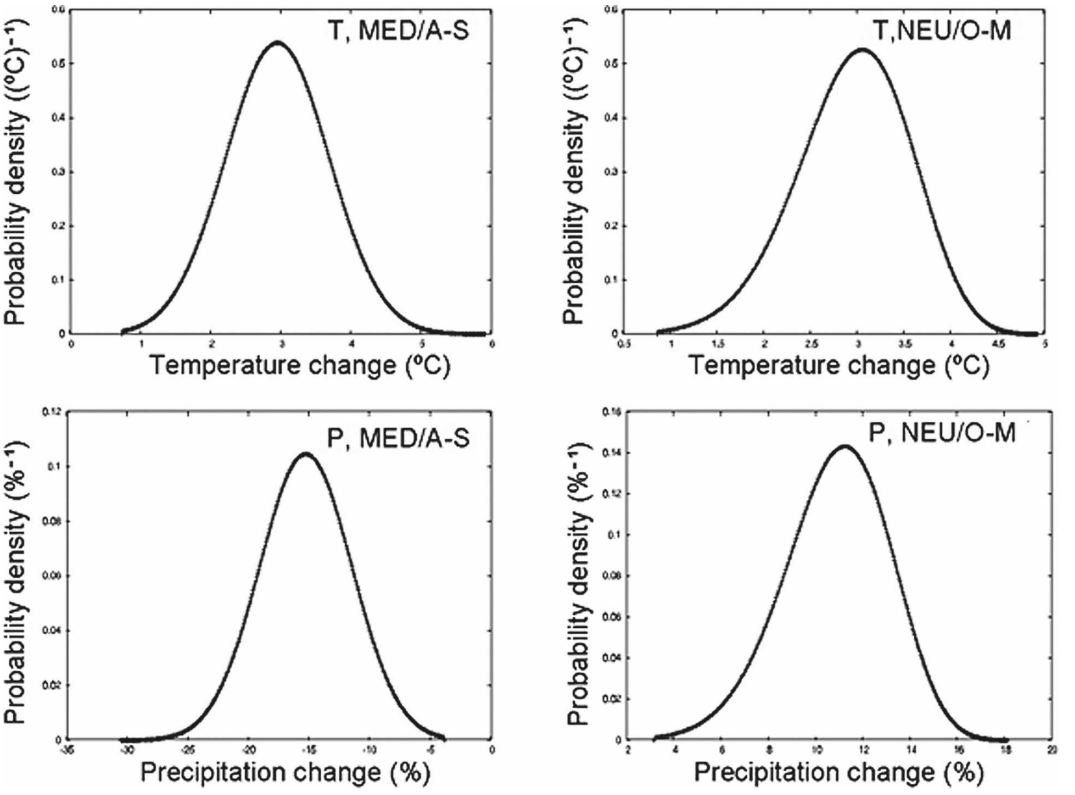

FIG. 8. Regional (top) temperature and (bottom) precipitation change PDFs for the MED A-S (AMJJAS) and NEU O-M (ONDJFM) cases obtained by applying the transfer function $F_{(T,P)}(\Delta Tg)$ to the ΔTg PDF of Fig. 7 without consideration of the uncertainty.

are applied to estimate the PDFs of temperature and precipitation change in the NEU ONDJFM and MED AMJJAS cases of section 3 using the GTC PDF of Fig. 7.

To apply our method, the GTC range of 0.5°–4°C is first divided into 350 equally spaced bins (i.e., 100 bins per degree). In fact, Fig. 7 shows the PDF based on values calculated at each bin from a normal PDF with mean at 2°C and standard deviation of 0.5°C. In the first type of application, when the uncertainty is not accounted for, the regional change PDF is simply obtained by multiplying the value of the GTC at each bin of the PDF by the transfer function $F_{(T,P)}(\Delta Tg)$ (with the proper unit normalization for temperature and precipitation). This defines a new range of change for the set of 350 bins. The probability density of a given bin is then retained for the "transformed" bins, thereby leading to a transformed PDF.

The results for temperature and precipitation in the NEU ONDJFM and MED AMJJAS cases are shown in Fig. 8. These PDFs can be compared with the "parent" GTC PDF of Fig. 7. For the MED AMJJAS case we first find a shift of the distribution, which retains a shape similar to that of the original GTC PDF. This is because the function $F_{(T,P)}(\Delta Tg)$ is a constant for both temperature and precipitation (see Tables 4 and 5). In the NEU ONDJFM case, however, we notice not only a shift, but also a deformation of the PDF, which becomes slightly asymmetric. This is because the function $F_{(T,P)}(\Delta Tg)$ has a decreasing trend with increasing GTC (see Tables 4 and 5). In addition, the transformed PDFs for the regional temperature changes are somewhat broader compared to the original GTC PDF, as evidenced by the fact that the standard deviation increases from 0.5°C in the GTC PDF to 0.61° and 0.73°C for the MED AMJJAS and NEU ONDJFM cases, respectively.

To include the effect of the uncertainty defined by the function $\sigma_{F,(T,P)}(\Delta Tg)$ we proceed as follows. First, we assume that the uncertainty at any given bin can be described by a normal PDF centered on the bin, having a standard deviation equal to $\sigma_{F,(T,P)}(\Delta Tg)$ and a median probability density value equal to the probability density of the GTC PDF at that bin. We then apply the transfer function $F_{(T,P)}(\Delta Tg)$ to the GTC PDF bin range in order to generate a new set of "transformed" bins for the regional changes. At each of the transformed bins we add the contribution to the probability

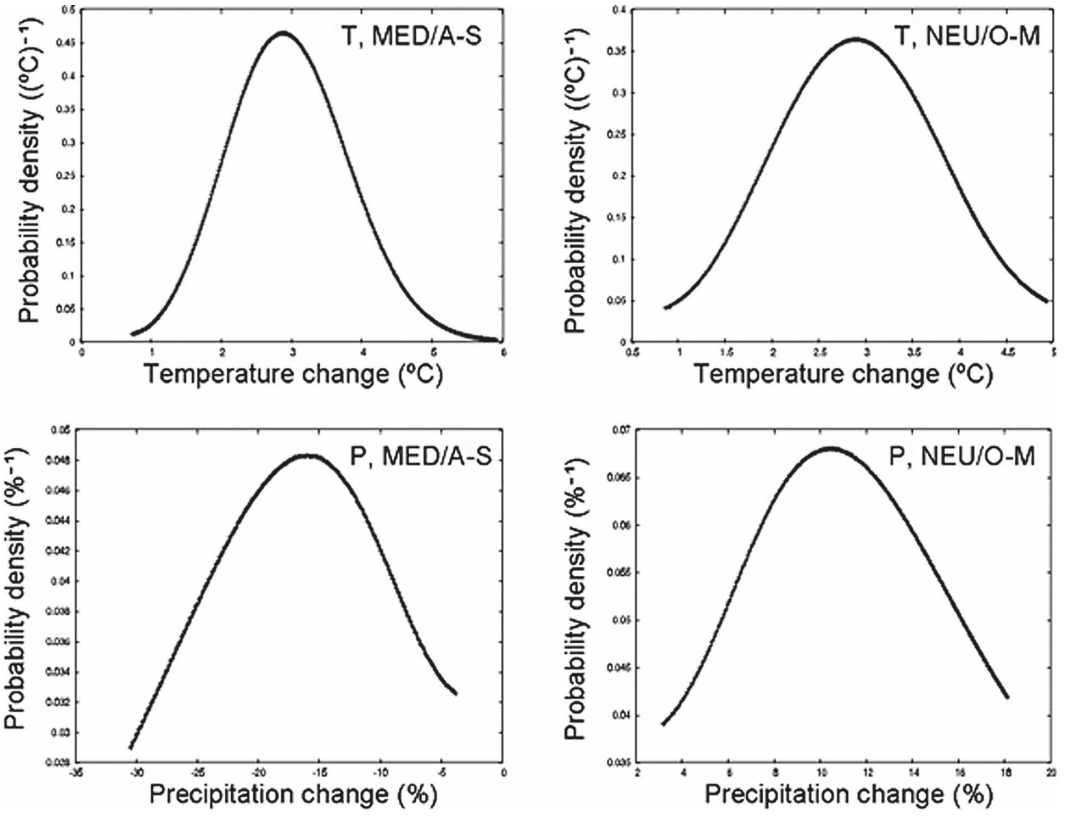

FIG. 9. Same as Fig. 8, but applying the transfer function $F_{(T,P)}(\Delta Tg)$ and the uncertainty function $\sigma_{F,(T,P)}(\Delta Tg)$.

density deriving from each PDF of all individual transformed bins. Finally, the resulting distribution is normalized in order to preserve the integral of the original GTC PDF.

The results from this procedure are shown in Fig. 9 and can be compared with the PDFs of Fig. 8 and the parent GTC PDF of Fig. 7. Note in Fig. 9 that the PDFs are defined only within the range of GTC used to derive the transfer and uncertainty functions; however, they could be extrapolated to wider GTC ranges with proper extrapolation of the functions $F_{(T,P)}(\Delta Tg)$ and $\sigma_{F,(T,P)}(\Delta Tg)$. An overall intercomparison of the PDFs in Figs. 8 and 9 shows that the addition of the uncertainty does not shift much the distributions, but affects the shape of the PDFs. In general, as can be expected, the PDFs become wider when the uncertainty is accounted for (for temperature the standard deviations increase from 0.5°C in the GTC PDF to 0.88° and 1.13°C in the MED AMJJAS and NEU ONDJFM cases, respectively). The smallest effect of the uncertainty is found for the temperature change in the MED AMJJAS case, when the value of $\sigma_{F,T}(\Delta Tg)$ is small (see Table 4). The largest effects are found in the case of the precipitation change PDFs, where in particular the tails of the distributions are modified. The transformed regional precipitation change PDFs cannot be considered Gaussian any more and are asymmetric with respect to the center of the distribution, with the large change portion of the distribution becoming effectively a straight line.

6. Summary considerations and discussion

In this paper simple equations are developed for regional climate change prediction and related uncertainties, where both these equations are expressed as a function of the GTC. The key underlying assumption in the use of Eqs. (1) and (2) is the remarkable scaling property that some surface climate variables show with respect to the global radiative forcing and GTC response. These properties hold especially well for temperature, giving Eqs. (1) and (2) a good level of robustness. For precipitation, the assumption holds, although in a less robust way, only for the cases in which the change signal is greater than the underlying uncertainty. It should be emphasized that, compared to the standard scaling approach, the method described here adds the estimate of the uncertainty due to intermodel and internal variability.

The recently developed MGME dataset (online at

http://www-pcmdi.llnl.gov) is used to derive the parameters of our equations. The methodology and the functioning of our equations are illustrated using temperature and precipitation change data over two subcontinental scale regions, northern Europe and the Mediterranean (as defined by Giorgi and Bi 2005). Parameter values are also presented, however, for temperature and precipitation change over 26 regions (from Giorgi and Bi 2005), encompassing all land areas of the globe (except for Antarctica). Finally, examples are shown of the application of Eqs. (1) and (2) to the generation of PDFs of regional climate change based on GTC PDFs.

This last application makes Eqs. (1) and (2) especially useful, because it allows us to estimate probabilities of regional climate change from the output of simple or intermediate complexity models. These models can in fact be run for very large ensembles encompassing much of the climate change parameter space. The approach presented in this paper thus provides a tool for probabilistic regional climate change prediction to complement existing methodologies (Räisänen and Palmer 2001; Giorgi and Mearns 2002, 2003; Stott and Kettleborough 2002; Forest et al. 2002; Tebaldi et al. 2005; Harris et al. 2006; Räisänen and Ruokolainen 2006; Stott et al. 2006).

Another attractive characteristic of our approach is that it provides a first-order estimate of regional climate change disentangling this estimate from the issue of scenarios and emission pathways, which has drawn much debate recently (e.g., Holtsmark and Alfsen 2005). Rather, the regional change estimates are only based on the GTC. Therefore, our equations would, for example, allow us to estimate the first-order regional response associated with given target GTC and GHG stabilization levels along with the associated uncertainty.

The limit of the approach evidently resides in the magnitude of the uncertainty, which in our case depends on the contributions of intermodel and internal variability. This uncertainty is a measure not only of the signal-to-noise ratio, but also of the validity of the *basic underlying* scaling assumption. We have seen that for temperature the uncertainty [as measured by the function $\sigma_{F,T}(\Delta\mathrm{Tg})$] is much smaller than the signal [as measured by the function $F_T(\Delta\mathrm{Tg})$] for all cases, so that the signals deriving from the use of Eqs. (1) and (2) can be considered robust. Conversely, for precipitation this is the case only for a much more limited number of cases, in which the precipitation change signal is especially large.

This method can be extended in various directions, first of all by considering the application to different variables (e.g., sea level pressure or circulation indicators) and/or higher-order statistics (e.g., variability and extremes). It would also be important to verify the scale limit for which the approach is valid. This paper focuses on the subcontinental scale, primarily because the resolution of the MGME models is highly variable, with some models still being run at rather coarse horizontal resolutions (4°–5°). It has been shown, however, that the surface climate change signal, in particular precipitation, shows substantial finescale structure in response to local forcings (e.g., topography; Gao et al. 2006), so that the scaling hypothesis underlying our approach needs to be verified at fine scales.

Another important issue concerns the effects of regional–local (aerosols, land-use change) versus global (GHG concentration) forcings. It can be expected that these different forcings might have different regional effects, which would in turn affect the scalability assumption underlying the validity of Eq. (1). The simulations analyzed here included both types of forcings (GHG and aerosol), which varied across different scenarios. Remarkably enough, although the aerosol facings are different in the different scenarios (Nakicenovic et al. 2000), the scalability assumption still seems to hold, which is suggestive of a dominant contribution of the GHG forcing for the experiments employed. These experiments however did not include all aerosols, so that aerosol effects might indeed be underestimated. In addition, they did not account for the effects of land-use change, which can also be especially important at the regional scale (Feddema et al. 2005). Therefore, the issue of regional versus global forcing needs to be carefully considered with more comprehensive model experiments.

The method developed in this paper hinges upon the availability of a sufficiently large number of intercomparable AOGCM simulations to develop meaningful calculations of the different parameters appearing in Eqs. (1) and (2), in particular the uncertainty functions. In this regard, the author would like to commend the MGME effort and recommends that such efforts be continued and further extended in the future to produce large enough ensembles of climate change simulations to improve our understanding and predictive capability of regional climate change.

Acknowledgments. I acknowledge the international modeling groups for providing their data for analysis, the Program for Climate Model Diagnosis and Intercomparison (PCMDI) for collecting and archiving the model data, the JSC/CLIVAR Working Group on Coupled Modeling (WGCM), and their Coupled Model Intercomparison Project (CMIP) and Climate Simula-

tion Panel for organizing the model data analysis activity, and the IPCC WG1 TSU for technical support. The IPCC Data Archive at Lawrence Livermore National Laboratory is supported by the Office of Science, U.S. Department of Energy. I also thank X. Bi for some technical support.

REFERENCES

Andronova, N. G., and M. E. Schlesinger, 2001: Objective estimation of the probability density function for climate sensitivity. *J. Geophys. Res.,* **106,** 22 605–22 612.

Feddemas, J. J., K. W. Oleson, G. B. Bonan, L. O. Mearns, L. E. Buja, G. E. Meehl, and W. M. Washington, 2005: The importance of land cover change in simulating future climates. *Science,* **310,** 1674–1678.

Forest, C. E., P. H. Stone, A. P. Sokolov, M. R. Allen, and M. D. Webster, 2002: Quantifying uncertainties in climate system properties with the use of recent climate observations. *Science,* **295,** 113–117.

Gao, X., J. S. Pal, and F. Giorgi, 2006: Projected changes in mean and extreme precipitation over the Mediterranean region from a high resolution double nested RCM simulation. *Geophys. Res. Lett.,* **33,** L03706, doi:10.1029/2005GL024954.

Giorgi, F., 2005a: Interdecadal variability of regional climate change: Implications for the development of regional climate change scenarios. *Meteor. Atmos. Phys.,* **89,** 1–15.

——, 2005b: Climate change prediction. *Climatic Change,* **73,** 239–265.

——, 2006: Climate change hot-spots. *Geophys. Res. Lett.,* **33,** L08707, doi:10.1029/2006GL025734.

——, and R. Francisco, 2000: Evaluating uncertainties in the prediction of regional climate change. *Geophys. Res. Lett.,* **27,** 1295–1298.

——, and L. O. Mearns, 2002: Calculation of average, uncertainty range, and reliability of regional climate changes from AOGCM simulations via the "Reliability Ensemble Averaging" (REA) method. *J. Climate,* **15,** 1141–1158.

——, and L. O. Mearns, 2003: Probability of regional climate change based on the Reliability Ensemble Averaging (REA) method. *Geophys. Res. Lett.,* **30,** 1629, doi:10.1029/2003GL017130.

——, and X. Bi, 2005: Updated regional precipitation and temperature changes for the 21st century from ensembles of recent AOGCM simulations. *Geophys. Res. Lett.,* **32,** L21715, doi:10.1029/2005GL024288.

Harris, G. R., D. M. H. Sexton, B. B. B. Booth, M. Collins, J. M. Murphy, and M. J. Webb, 2006: Frequency distributions of transient regional climate change from perturbed physics ensembles of general circulation model simulations. *Climate Dyn.,* **27,** 357–375.

Holtsmark, B. J., and K. H. Alfsen, 2005: PPP correction of the IPCC emission scenarios—Does it matter? *Climatic Change,* **68,** 11–19.

Houghton, J. T., Y. Ding, D. J. Griggs, M. Noguer, P. J. van der Linden, X. Dai, K. Maskell, and C. A. Johnson, Eds., 2001: *Climate Change 2001: The Scientific Basis.* Cambridge University Press, 881 pp.

Kittel, T. G. F., F. Giorgi, and G. A. Meehl, 1997: Intercomparison of regional biases and doubled CO_2-sensitivity of coupled atmosphere-ocean general circulation model experiments. *Climate Dyn.,* **14,** 1–15.

Mastrandrea, M. D., and S. H. Schneider, 2004: Probabilistic integrated assessment of "dangerous" climate change. *Science,* **304,** 571–575.

Mitchell, J. F. B., T. C. Johns, M. Eagles, W. J. Ingram, and R. A. Davis, 1999: Towards the construction of climate change scenarios. *Climatic Change,* **41,** 547–581.

Mitchell, T. D., 2003: Pattern scaling: An examination of the accuracy of the technique for describing future climates. *Climatic Change,* **60,** 217–242.

Nakicenovic, N., and Coeditors, Eds., 2000: *IPCC Special Report on Emission Scenarios.* Cambridge University Press, 599 pp.

New, M., M. Hulme, and P. Jones, 2000: Representing twentieth-century space–time climate variability. Part II: Development of 1901–96 monthly grids of terrestrial surface climate. *J. Climate,* **13,** 2217–2238.

Räisänen, J., and T. N. Palmer, 2001: A probability and decision-model analysis of a multimodel ensemble of climate change simulations. *J. Climate,* **14,** 3212–3226.

——, and L. Ruokolainen, 2006: Probabilistic forecasts of near-term climate change based on a resampling ensemble technique. *Tellus,* **58A,** 461–472.

——, and Coauthors, 2004: European climate in the late twenty-first century: Regional simulations with two driving global models and two forcing scenarios. *Climate Dyn.,* **22,** 13–31.

Stott, P. A., and J. A. Kettleborough, 2002: Origins and estimates of uncertainty in predictions of twenty-first century temperature rise. *Nature,* **416,** 723–726.

——, ——, and M. R. Allen, 2006: Uncertainty in continental-scale temperature predictions. *Geophys. Res. Lett.,* **33,** L02708, doi:10.1029/2005GL024423.

Tebaldi, C., R. L. Smith, D. Nychka, and L. O. Mearns, 2005: Quantifying uncertainty in projections of regional climate change: A Bayesian approach to the analysis of multimodel ensembles. *J. Climate,* **18,** 1524–1540.

Webster, M., and Coauthors, 2003: Uncertainty analysis of climate change and policy response. *Climatic Change,* **61,** 295–320.

Wigley, T. M. L., and S. C. B. Raper, 2001: Interpretation of high projections for global-mean warming. *Science,* **293,** 451–454.